The spin evolution of accreting and radio pulsars in binary systems

Nielsen, A.B.

CHAPTER 5

A study of timing stability of Black Widow pulsars

We study the timing stability of three black widow pulsars, both in terms of long-term variation as well as shorter-term changes in their orbital parameters. The erratic timing behaviour and radio eclipses of the first two black widow pulsar systems discovered (PSRs B1957−20 and J2051+0827) was assumed to be representative for this class of pulsars. With several new black widow systems added to this population in the last decade, there are now several systems known that do not show the typical orbital timing variations or radio eclipses. We present timing solutions using 7−8 yrs of observations, using data from four of the European Pulsar Timing Array telescopes for PSRs J0023+0923, J2214+3000 and J2234+0944, and confirm that these pulsars do not show any significant variations over our observing time span, both in terms of secular or orbital parameters. Our results from the long-term timing of these pulsars provide several new or improved parameters compared to earlier work. We discuss our results regarding the stability of these pulsars, and the stability of the class of black widow pulsars in general, in context of the binary parameters, and discuss the potential of the Roche lobe filling factor of the companion star being an indicator of stability of these systems.

A. Bak Nielsen, G. Janssen, G. Shaifullah, J. Verbiest, L. Guillemot, B. Stappers, A. Possenti, and the EPTA collaboration

Paper in prep.

5.1 Introduction

The first radio pulsar was discovered in 1967 by Jocelyn Bell (Hewish et al. 1968) and since then more than 2600 radio pulsars have been found (Manchester 2017). Those $\sim$ 2600 radio pulsars include both isolated pulsars and pulsars in binary systems, and slow and millisecond pulsars (MSPs). The millisecond pulsars are thought to have formed through the recycling scenario, which implies that MSPs have spun up and decreased their magnetic field through X-ray binary evolution (Alpar et al. 1982; Bhattacharya & van den Heuvel 1991). Pulsars are spun up in binary systems through accretion, which transfers angular momentum onto the pulsar. During the X-ray pulsar phase, the magnetic field of the pulsar decreases (Chen et al. 2013). When accretion stops, the newly formed MSPs in binary systems include the so called 'spiders'. These are the 'redback' pulsars (RBPs), which have companion star masses of $M_2 \simeq 0.1 - 0.4\,M_\odot$, and the 'black widow' pulsars (BWPs), with $M_2 \ll 0.1\,M_\odot$ (Chen et al. 2013). The low mass companions of BWPs are often thought to be degenerate stars, similar to brown dwarfs (see section 4.4 in Lazaridis et al. (2011)). The companions of RBPs are non-degenerate stars, as suggested by a few cases where the optical counterpart was discovered (Roberts 2011, 2013). The fate of the companion star in the BWP systems is unclear. However, one discussed scenario is that the companion could be fully ablated, creating an isolated MSP. Alternatively, tidal effects could play a significant role in destroying the companion (Stappers et al. 1998; Chen et al. 2013).

Since the discovery of PSR B1957+20 and J2051−0827, the population of BWPs and RBPs have increased greatly with recent surveys, using either radio surveys which were optimised to find MSPs, or targeted surveys at high energies using e.g. *Fermi*. At least 30+ MSPs were found using such surveys over the past few years (Roberts 2011). The two original BWP systems show eclipses of the radio emission from the pulsar, which are thought to originate from the companion star and be broadened by material being ablated off of the companion star by a strong pulsar wind (Fruchter et al. 1988; Stappers et al. 1996; Chen et al. 2013). The BWPs are, due to the ablated material, often complicated systems to use for precision timing. The companion stars are often bloated, and they exert small torques on the system, which will then cause small changes in the orbit. The changes in the orbit increase the number of parameters that is required in timing models, and their variability could reduce the sensitivity of the timing solution to the gravitational wave (GW) signals (Bochenek et al. 2015). By observing multiple stable pulsars in different parts of the sky, an array of pulsars, and cross-correlating the timing residuals from the different pulsars, it should be possible to obtain the sensitivity to measure the expected quadrapolar signature of a GW. This is the general idea behind the pulsar timing arrays (PTAs) (Lentati et al. 2015).

With new BWPs being discovered, Bochenek et al. (2015) tested the feasibility of using BWPs in the pulsar timing arrays, by testing if fitting for multiple orbital frequency derivatives was significantly reducing the sensitivity to the GW signal. Bochenek et al. (2015) used simulated data sets of five different pulsars to constrain how sensitive to a GW signal a timing solution would be, if several orbital period derivatives were fitted for. They found that the sensitivity to the GW signals were

not reduced significantly, partly due to GW signals spanning several years and the typical BWP orbit spans 2 to 20 hr. It was thus concluded that some BWPs could be used in pulsar timing arrays, and PSR J0610−2100 is already used by the PTAs (Desvignes et al. 2016). There are three other BWPs that are stable and which are candidates for the PTAs: PSRs J0023+0923, J2214+3000 and J2234+0944. All three are currently observed by the North American Nanohertz Observatory for Gravitational Waves (NANOGrav) (Arzoumanian et al. 2018) and the European Pulsar Timing Array (EPTA) (this work).

PSR J0023+0923 was discovered with the Green Bank Telescope (GBT) through the survey of *Fermi* γ-ray sources (Hessels et al. 2011). PSR J0023+0923 is a millisecond pulsar with a spin period of $\sim$3 ms, an orbital period of about 3.3 hr and a companion mass of 0.016 $M_\odot$. The optical counterpart to PSR J0023+0923 was discovered by Breton et al. (2013) with the *Gemini North* telescope. By combining measurements of the filling factor with the estimated distance from the dispersion measure value they inferred that the companion star never fills its Roche lobe. Their results show that when taking the small filling factor into account, the companion star could be as small as 0.05 $R_\odot$. PSR J0023+0923 has also been observed in X-rays, but no pulsations were detected (Ransom et al. 2011).

PSR J2214+3000 was discovered with the GBT, searching for radio pulsars among unassociated sources in the *Fermi*-LAT list of sources (Ransom et al. 2011). It was discovered to be a BWP system, with a low mass companion ($\sim$ 0.02 $M_\odot$) and an orbital period of about 10 hr. The companion star of PSR J2214+3000 was detected in optical by Schroeder & Halpern (2014)

PSR J2234+0944 has an orbital period of about 10 hr, with a companion star of $\sim$0.015 $M_\odot$, and a spin period of $\sim$3.36 ms. The pulsar was found with the Parkes telescope as a part of the search for radio sources that could be associated with unidentified *Fermi*-LAT sources (Ray et al. 2012).

The three pulsars have all been observed in γ-ray and they all show γ-ray pulsations[1] (Ransom et al. 2011).

In this chapter we present updated timing solutions for the three BWPs J0023+0923, J2214+3000 and J2234+0944. In section 5.2 we present the observations of the three BWPs, in section 5.3 we present our timing solutions and in section 5.4 we discuss the stability of these pulsars and compare their properties with other BWPs.

[1] `https://confluence.slac.stanford.edu/display/GLAMCOG/Public+List+of+LAT-Detected+Gamma-Ray+Pulsars`

5.2 Observations

The data in this chapter consists of time of arrivals (TOAs), derived from data from four telescopes that are all part of the European Pulsar Timing Array (EPTA). The EPTA is a collaboration of scientists working with five different telescopes around Europe, the Westerbork Synthesis Radio Telescope (WSRT) in the Netherlands, the Effelsberg Radio Telescope (EFF) in Germany, the Lovell Radio Telescope (JBO) in the UK, the Nançay Radio Telescope (NRT) in France and The Sardinia Radio Telescope (SRT) in Italy (Desvignes et al. 2016). As SRT is a more recent telescope, data from this telescope is not used in this chapter. The aim of the EPTA, like other PTAs, is to enable the detection of the stochastic gravitational wave background (Lee et al. 2011; Desvignes et al. 2016). The three data sets for PSR J0023+0923, J2214+3000 and J2234+0944 respectively span about 7.5, 8 and 7 years of data, see Fig. 5.1. The data used is from several pulsar recording instruments, see Table 5.1 (Karuppusamy et al. 2008; Desvignes et al. 2011; Lazarus et al. 2016; Shaifullah et al. 2016; Guillemot et al. 2016).

The data was collected using different pulsar timing backends (see table 5.1) and was recorded using coherent dedispersion and online folding. Specific parts of the data that were affected by RFI were zapped using standard PSRCHIVE tools. The cleaned data was frequency and time scrunched, meaning the time and frequency of the data cubes were collapsed. For PSR J0023+0923, some observations were taken with a total integration time of several hours, to cover the full orbital period. We split observations that were more than 1 hr long, into smaller subsets of 30 min each, to avoid smearing due to a non-optimal folding solution. The data for PSR J0023+0923 was also refolded, to correct for orbital signatures in the long observations of this source.

The TOAs were created by cross-correlating the time integrated and frequency scrunched data using the total intensity profile analytical templates, which were constructed by fitting von Mises functions to the high signal to noise pulse profiles, using the `paas` tool. The TOAs were generated using the `pat` tool[2], which creates TOAs with a Fourier domain with Markov chain Monte Carlo algorithm (van Straten et al. 2012). Our standard procedure of integrating over the full available bandwidth was insufficient for the NUPPI data from NRT. Since the ISM is not only magnetised and ionised, but is also a turbulent medium and very inhomogeneous, the irregularities cause the observed radio emission to fluctuate over different bandwidths and timescales, which lead to interstellar scintillation (Tielens 2009; Lorimer & Kramer 2012). This is strongly affecting the TOAs derived from the NUPPI backend of NRT, with its large bandwidth of 512 MHz, showing strong scintillation for the PSR J2234+0944, as shown on Fig. 5.2, and less strong scintillation for PSR J0023+0923 and J2214+3000. We refer the calculated TOA to the center of the observing band. However, in case of strong scintillation, this may lead to an apparent time-offset in the calculated TOA due to the reference

[2]See also `psrchive.sourceforge.net`

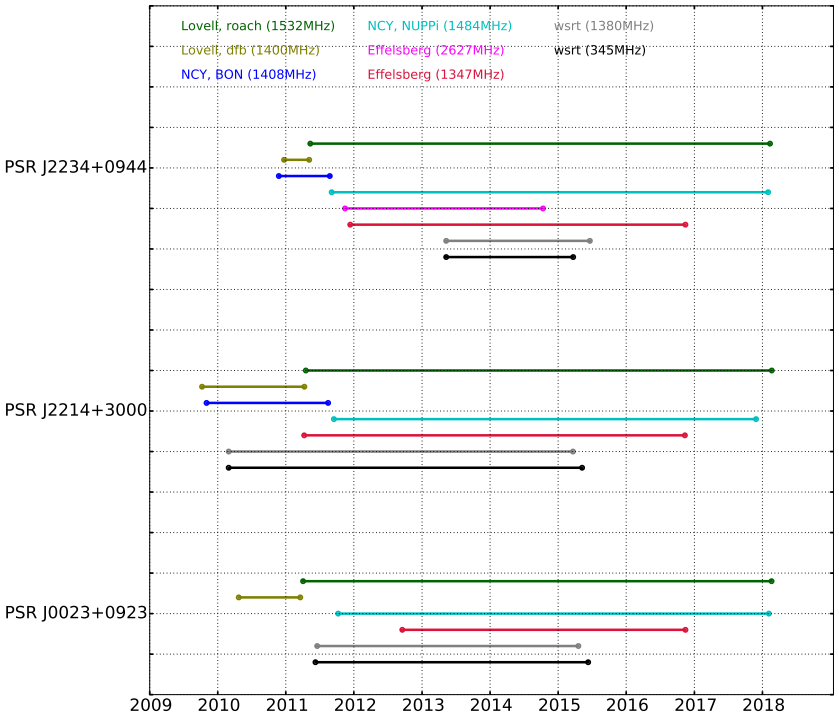

Figure 5.1: Plot showing the timing baselines per backend for the three BWPs discussed in this chapter. The colours correspond to backend and observing frequnecy band combinations. The dark green lines represent the time span covered by the ROACH-based backend, observing at a centre frequency of 1532 MHz, and the light green line represents the AFB at 1400 MHz, both at the Lovell radio telescope. The dark blue line represents the BON backend at 1408 MHz, and the light blue the NUPPI backend at 1404 MHz, both at the Nançay Radio Observatory. The pink and red lines represent timing spans of the PSRIX backend at 2627 and 1347 MHz, respectively at the Effelsberg 100-m radio telescope. Finally, the grey and black lines represent timing baselines for the PuMa-II backend at the Westerbork Synthesis Radio Telescope. More details for the backends and telescopes can be found in the text and Table 5.1.

frequency not reflecting the data itself. To correct the TOAs for scintillation, we divided the bandwidth in two, which for PSR J0023+0923 and J2214+3000 improved the timing solution. For PSR J2234+0944 only splitting the bandwidth in two improved half of the band, but the other half of the band still showed variations due to scintillation. We thus split the band in half again. This process resulted in TOAs that were only marginally affected by scintillation. We adopt this workaround for this work, reserving a full 2D-template matching method for future work.

The TOAs were measured with reference to a local clock at each observatory, and corrected to the Solar system barycentre using the NASA-JPL DE421 planetary ephemerides (Folkner et al. 2009). The reference clock used was the Terrestrial Time standard, which is derived from the "Temps Atomique International" time standard, TT(TAI) (Hobbs et al. 2006) and the ELL1 (T2) model was used in fitting the TOAs (Lange et al. 2001). Data sets generated by different telescopes were aligned by using constant offsets (JUMPS; following the procedure as described in Verbiest et al. (2016)) and a few clock or timing offsets were applied where necessary.

`Tempo2`[3] error scaling factors were calculated for each telescope backend, using the timing model derived in the previous steps and taking the square root of the reduced χ^2, giving a `T2EFAC` vale. The `T2EFAC` value corrects the weight of the data by rescaling the error bars to correct for under estimation.

5.3 Results

We found a stable timing solution to the three pulsars PSR J0023+0923, J2214+3000 and J2234+0944 over the time span 7−8 years, using data from four of the EPTA telescopes. In table 5.2 the best fit timing solutions to the three pulsars are shown and in Fig. 5.3 the timing residuals of the three BWPs are shown.

5.3.1 New parameter measurements

For the timing solution we have used the ELL1 model, which is valid only for small eccentricities. The ELL1 model use Laplace parameters, $\epsilon_1 = e\,sin(\omega)$ and $\epsilon_2 = e\,cos(\omega)$, instead of the eccentricity and omega. For low eccentricities the location of periastron is not well defined and a strong correlation between ω and T_0 occur. This leads to very large uncertainties in the estimate of χ^2 of these parameters. By using the ELL1 model this is corrected (Lange et al. 2001). In this chapter we introduce and measure a first order derivative of the dispersion measure ($\dot{DM}$) for PSR J2214+3000, of $3.5(5)\times10^{-4}$cm^{-3} pc yr^{-1}. This accounts for the DM variations we show in Fig. 5.4 (for more details see section 5.3.2). We measure ϵ_1 and ϵ_2, which are effectively the eccentricity, of the three pulsars. The eccentricity is given by $e = \sqrt{\epsilon_1^2 + \epsilon_2^2}$ and the eccentricities of the pulsars are thus $e = 4.8(10)\times10^{-5}$, $e = 3.0(11)\times10^{-5}$, $e = 5.2(31)\times10^{-6}$ respectively for PSR

[3]Throughout this work `Tempo2` version 2014.2.1 was used.

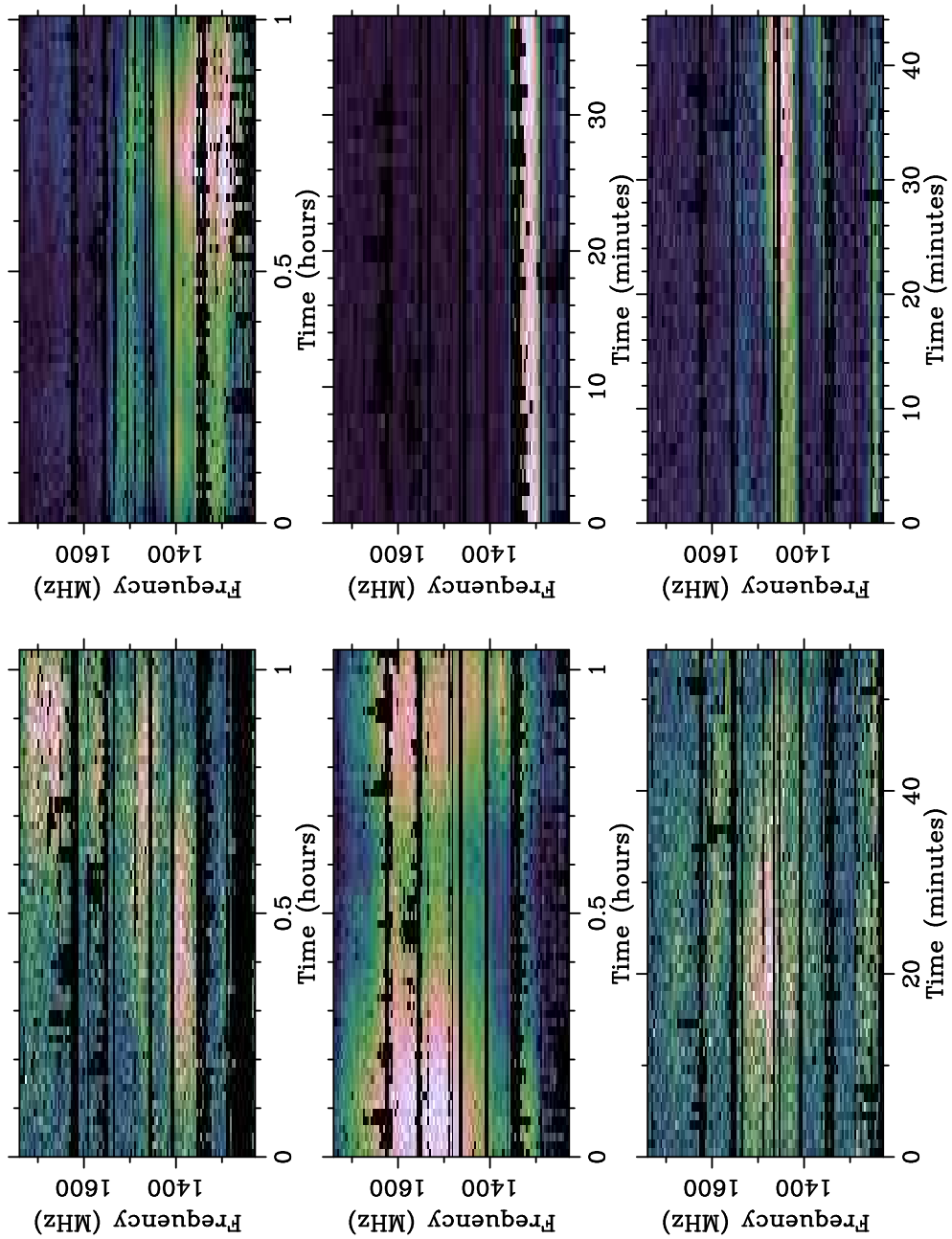

Figure 5.2: On the dynamical spectra, the scintillation over bandwidth is clearly seen for the pulsar J2234+0944. The variation affects the precision timing of the Nançay data with the NUPPI backend.

Table 5.1: Telescope backends, centre frequency, bandwidth, and number of TOAs for the different pulsars. The four telescopes used are a part of the EPTA and they are the Westerbork telescope (WSRT), Effelsberg, Nanạy, and Lovell at Jodrell Bank. *The data from Nançay, NUPPI, is affected by scintillation, and the frequency bands have thus been split into smaller bands, of 256MHz for PSR J0023+0923 and J2214+3000, for PSR J2234+0944 we have split the band in three, so we have one band of 256MHz and two bands of 128MHz.

Telescope (Backend)	f_c (MHz)	BW (MHz)	No. of TOAs (J0023+0923)	No. of TOAs (J2214+3000)	No. of TOAs (J2234+0944)
WSRT (PuMaII)	345	70	55	51	27
	1380	160	36	61	44
Efflsberg (PSRIX)	1347.5	200	59	25	31
	2627	200	-	-	27
Nançay (NUPPI)	1484	512/256/128*	784	193	486
Nançay (BON)	1408	128	-	108	31
Lovell (DFB)	1400	16	25	108	48x
Lovell (ROACH)	1532	400	115	126	147

Table 5.2: Timing solutions for the three BWPs discussed in this chapter; PSRs J0023+0923, J2214+3000 & J2234+0944. In the timing solutions we used TT(TAI) as the Clock correction procedure, DE421 as the Solar system ephemeris model and T2(ELL1) as the binary model.

Fit and data-set			
Pulsar name	J0023+0923	J2214+3000	J2234+0944
MJD range	55309.6—58167.8	55112.9—58168.8	55524.7—58159.5
Data span (yr)	7.83	8.37	7.21
Number of TOAs	1074	660	841
Rms timing residual (μs)	3.7	5.3	1.8
Reduced χ^2 value	1.0	1.0	1.0
Measured Quantities			
Right ascension, α (hh:mm:ss)	00:23:16.877776(19)	22:14:38.852766(18)	22:34:46.853751(6)
Declination, δ (dd:mm:ss)	+09:23:23.8623(7)	+30:00:38.1968(4)	+09:44:30.25618(18)
Pulse frequency, ν (s^{-1})	327.8470154891365(8)	320.592287390235(3)	275.7078283945942(6)
First derivative of pulse frequency, $\dot{\nu}$ (s^{-2})	$-1.22767(3)\times10^{-15}$	$-1.51364(6)\times10^{-15}$	$-1.527891(19)\times10^{-15}$
Dispersion measure, DM ($cm^{-3}pc$)	14.322(3)	22.565(4)	17.8292(9)
First derivative of dispersion measure, $\dot{DM}$ ($cm^{-3}pc\,yr^{-1}$)		$3.5(5)\times10^{-4}$	
Proper motion in right ascension, $\mu_\alpha \cos\delta$ ($mas\,yr^{-1}$)	$-12.79(16)$	20.64(10)	7.08(6)
Proper motion in declination, μ_δ ($mas\,yr^{-1}$)	$-5.0(4)$	$-1.35(16)$	$-32.50(10)$
Orbital period, P_b (d)	0.13879914697(13)	0.4166329525(3)	0.4196600431(3)
Projected semi-major axis of orbit, x (lt-s)	0.03484151(19)	0.0590819(6)	0.06842971(12)
First derivative of orbital period, $\dot{P}_b$	$-1.23(7)\times10^{-12}$		$4.7(17)\times10^{-13}$
First derivative of x, $\dot{x}$ (10^{-12})		$-1.7(7)\times10^{-14}$	
TASC (MJD)	55186.1136004(7)	55094.1380394(7)	55517.4822997(3)
EPS1 (ϵ_1)	$4.7(11)\times10^{-5}$	$3.0(11)\times10^{-5}$	$-4.8(31)\times10^{-6}$
EPS2 (ϵ_2)	$-1.0(10)\times10^{-5}$	$-3.7(118)\times10^{-6}$	$-2.0(31)\times10^{-6}$
Upper Limits			
Parallax, π (mas)	0.4(4)		
First derivative of x, $\dot{x}$ (10^{-12})	$4.1(32)\times10^{-15}$		
Set Quantities			
Epoch of frequency, position and DM determination (MJD)	56738	56640	56842

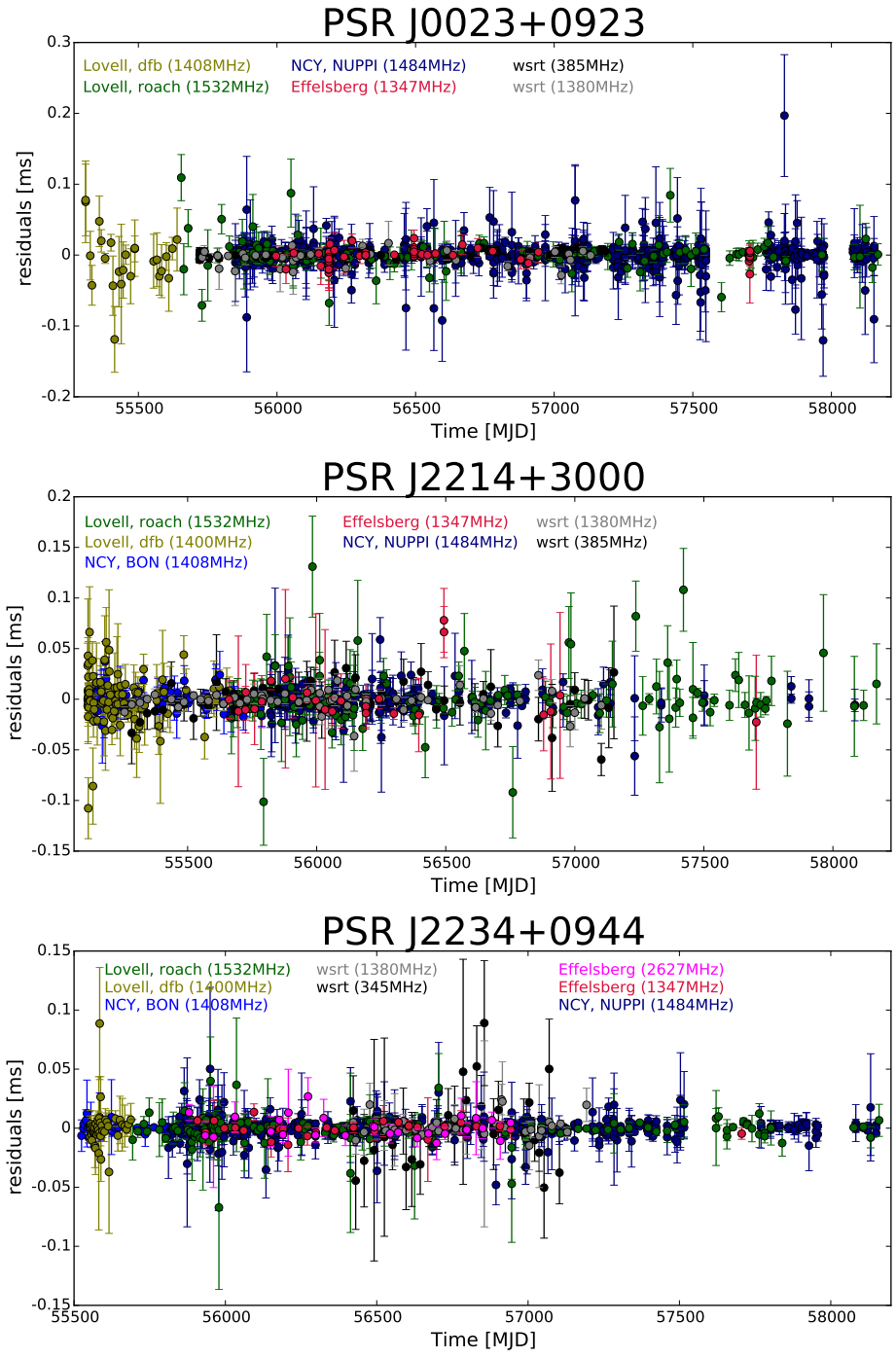

Figure 5.3: The timing residuals of PSRs J0023+0923, J2234+0944 and J2214+3000 after fitting the timing models presented in Table 5.2. The residuals show stability over the collective length of all the observations.

J0023+0923, J2214+3000 and J2234+0944. The eccentricity of J0023+0923 is significant, however, for the two other pulsars they are counted as marginally significant and an upper limit. Any value below a 2σ significance has been set to be an upper limit, and values around or a bit more than a 2σ significance have been set to be marginally detected, in table 5.2. The upper limits stated in table 5.2 are not used in the final timing solution. We found an upper limit on the parallax of PSR J0023+0923, of PX$\leq$0.4(4) mas, which differs from a previous measurement of 0.93(15) mas (Arzoumanian et al. 2018). We further find a marginal detection of the first order derivative of the semi major axis, of $-1.7(7)\times10^{-14}$ for PSR J2214+3000 and an upper limit for the first order derivative of the orbital period, of $4.7(17)\times10^{-13}$ for PSR J2234+0944. Furthermore, we found a significant value of $\dot{P}_b$ for PSR J0023+0923, of $-1.23(7)\times10^{-12}$, which is significantly different from previous measurements (see section 5.4.2) (Arzoumanian et al. 2018).

5.3.2 Dispersion Measure

We also tested for DM variations along the lines of sight to the three pulsars. The effects on the DM are inversely proportional to the observing frequency, and are therefore more easily detectable at lower frequencies. In Fig. 5.4 we see an example of the DM variations in PSR J2214+3000. The DM measurements on Fig. 5.4 were created by fitting the DM and first order derivative of DM to segments of data that were around 100 days long. The top panel of Fig. 5.4 show the total frequency range of the WSRT data, where we do not detect any DM variations. However, if we only look at the low frequency of the WSRT data, lower panel, we see DM variations. We here detected a first order DM derivative of $3.5(5)\times10^{-4}\mathrm{cm}^{-3}\,\mathrm{pc\ yr}^{-1}$. For PSRs J0023+0923 and J2234+0944 we did not detect any DM variations.

5.4 Discussion

In the following section we will discuss some of the features that the three sources show and relate these to the long term stability of the three BWPs. We will furthermore compare the properties of stable and unstable BWPs.

5.4.1 Stability

The first BWP found, PSR B1957+20, is unstable over long durations of time, implying that it was not possible to create a valid timing solution for more than a few months to maybe a year (Arzoumanian et al. 1994). The pulsar also showed radio eclipses due to the bloated companion and material surrounding the companion, which is blocking the line of sight towards the pulsar. The second BWP found, PSR J2051−0827, showed similar behavior, including timing solutions that were only stable for short periods of time, of about 3 yrs (Lazaridis et al. 2011; Shaifullah et al. 2016). There are several other BWPs known that show variations. Amongst these is PSR J1731−1847, which shows clear radio eclipses similar to the eclipses seen in the first two observed BWPs. PSR J1731−1847 also shows

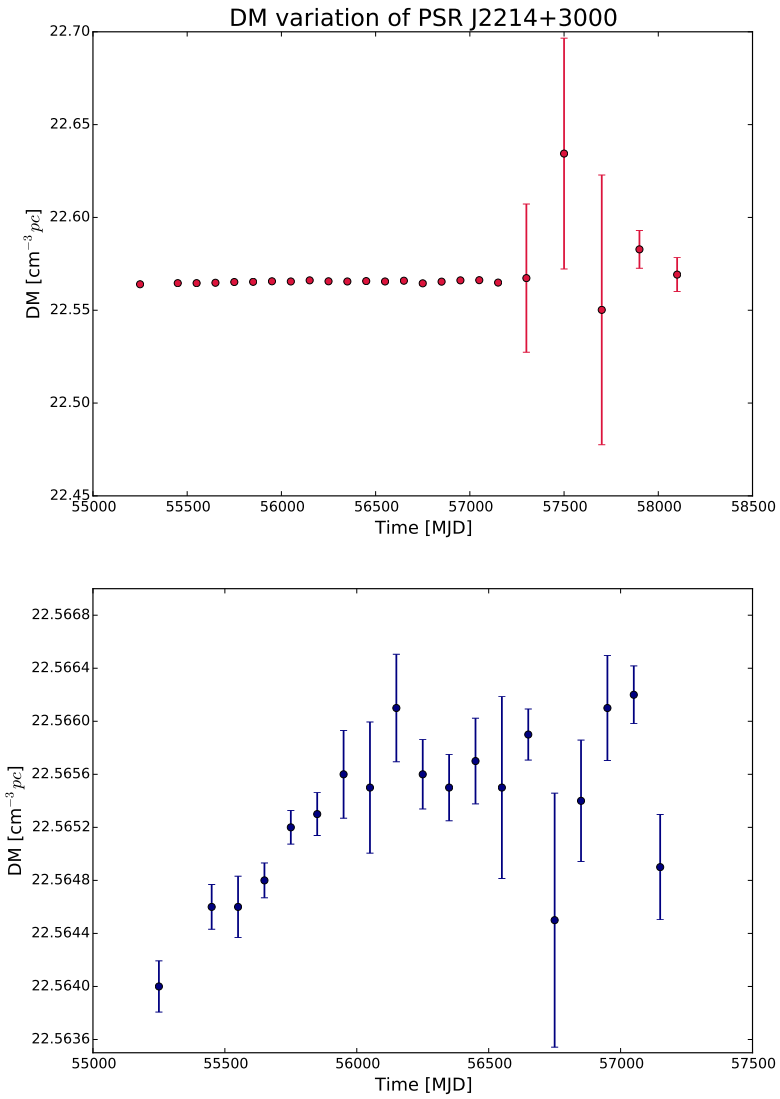

Figure 5.4: Dispersion measure variations are evident for PSR J2214+3000. The dispersion measure derivative in the data is clearly visible in the low frequency data, as shown by the DM time-series derived from those data plotted in the lower panel. The top panel include both high and low frequency data, whereas the lower panel only include 345 MHz data, from the Westerbork telescope.

orbital period variations on relatively short timescales, ∼3 yrs, comparable to PSR B1957+20 and J2051−0827 (Bates et al. 2011; Ng et al. 2014). The three BWPs in this chapter are very different from the first two BWPs. None of the three BWPs show radio eclipses and it is possible to find a coherent timing solution for each of the three systems that is valid over a 7−8 year period. Furthermore, there is one other BWPs system, aside from the three pulsars in this chapter, that show a stable timing solution. This is PSR J0610−2100, which was already included in the EPTA data set (Desvignes et al. 2016).

5.4.2 Different orbital period derivatives

In section 5.3 we mentioned that there was a difference between the value presented in Arzoumanian et al. (2018) and our measurement of the orbital period derivative, $\dot{P}_b$, of PSR J0023+0923. Orbital period changes are due to e.g. gravitational wave emission, acceleration of the binary system, mass loss from the system or tidal interactions in the system (see e.g. Lorimer & Kramer (2012)). One of the differences between this work and the work by Arzoumanian et al. (2018) is that the aim of this chapter is to understand the physical difference of the stable and unstable BWPs, whereas the aim of Arzoumanian et al. (2018) is to reduce the white noise of an array of pulsars, in order to be sensitive to an eventual GW signal. We therefore believe the difference in the parameter can be explained by a different approach towards including additional orbital derivatives in the fitting procedure.

5.4.3 Eclipses

We examined our data sets for the three pulsars for eclipses, and do not find any evidence for radio eclipses for any of the three pulsars at any of our observed frequencies. This indicates that there is indeed not enough material around the companion to create the eclipses, as is also suggested for J0023+0923 from X-ray observations by Gentile et al. (2014). The lack of radio eclipses can be an indication that the companion stars are not filling their Roche lobe (see section 5.4.4).

5.4.4 Roche lobe filling factors

The companion stars for the first two black widow pulsars, B1957+20 and J2051−0827, are suggested to be Roche lobe filling (Stappers et al. 2001; van Kerkwijk et al. 2011). This means that the outer layers of the companion star are less gravitationally bound to the star and it is thus easier to expel material from, or ablate the companion star. This is one of the essential details of the geometry of the BWPs, as it is the ablated material that causes the radio eclipses (van Kerkwijk et al. 2011). The Roche lobe filling factors for PSR B1957+20 and J2051−0827 are about 0.9, i.e. the Roche lobe is almost filled. The filling factors are determined from fitting the optical light curve of the companion stars (Stappers et al. 2001; Reynolds et al. 2007; van Kerkwijk et al. 2011). The same applies to the recently

found BWP J1810+1744, which also shows radio eclipses and instabilities (Breton et al. 2013; Polzin et al. 2018).

The filling factor of the companion star of PSR J0023+0923 was found to be ∼0.3, from fitting the light curve of the companion star, which means that the companion star is far from filling its Roche lobe (Breton et al. 2013). Binary systems where the companion is not filling its Roche lobe typically show less variability in their orbits and a consequence for the system may thus be that the BWP system PSR J0023+0923 is a stable system (Breton et al. 2013). If the Roche lobe of a BWP system is not filled, eclipses would not be expected, which coincide with what is observed for PRS J0023+0924, J2214+3000 and J2234+0944. It is thus possible that the filling factors could be used as an indicator of whether systems are stable or unstable.

5.4.5 PSR J2234+0944 as a possible transitional system

Transitional millisecond pulsars are a relatively new class of binary pulsars, that show changes between emitting in radio and X-ray, and are believed to switch states between having an active accretion disc and an inactive or no accretion disc (Archibald et al. 2009). Since the first transitional millisecond pulsar, PSR J1023+0038, was discovered to switch states, two more have been found, and all three systems are RBPs (Papitto et al. 2013; Bassa et al. 2014; Roy et al. 2015). The companion stars of BWPs and RBPs are very different, as RBPs have non-degenerate companions with a higher mass than the semi-degenerate companions of BWPs (Chen et al. 2013). However, variations in their orbit and that some systems show radio eclipses are shared between the BWPs and the transitional systems (Fruchter et al. 1988; Stappers et al. 1996; Archibald et al. 2009; Papitto et al. 2013; Chen et al. 2013; Roy et al. 2015). Torres et al. (2017) suggested that the pulsar PSR J2234+0944 could be a potential transitional system, based on variations in the γ-ray spectrum, which is similar to what is seen in the transitional millisecond pulsar PSR J1227−4853. However, PSR J2234+0944 has a timing solution that is stable over 8 yrs, with no obvious irregularities, and no obvious eclipses. This system is thus different from the variable transitional systems, which would seem to suggest that PSR J2234+0944 is not a transitional system.

5.5 Conclusions

We studied three BWPs, PSR J0023+0923, J2234+0944 and J2214+3000, all of which showed a different behaviour than the two first discovered pulsars PSR B1957+20 and J2051−0827. The first two discovered pulsars show unstable timing solutions, where it is only possible to create a stable solution over a few months to years. We present timing solutions for PSR J0023+0923, J2214+3000 and J2234+0944, that are stable over a time span of 7−8 yrs. Compared to earlier work, our timing solution is sensitive to a few new parameters and we present upper limits

on other parameters: we find an upper limit of the parallax of PSR J0023+0923 which differs significantly from a previous measurement (Arzoumanian et al. 2018). Furthermore we set limits and introduce significant measurement of the eccentricity of the BWPs in this chapter. We also measure an orbital period derivative for PSR J0023+0923, of $-1.23(7)\times10^{-12}$, which also differs significantly from previous measurements (Arzoumanian et al. 2018). The BWPs in this study are all stable, and we discuss their properties to find out what causes these differences in timing behaviour. It is possible that it is due to their companion star not filling the Roche lobe. This would make the systems more tightly bound, resulting in a cleaner system with less material to interfere with, or affect the radio signal and the orbital parameters. Since the three pulsars show stability over long timescales it is possible to use the systems as a part of the pulsar timing arrays. For future work we will further fine tune our fitting procedure, which will improve the measurement of all timing parameters. It furthermore remains to be seen if the lack of stability in some of these gravitationally tightly bound systems are tied to specific high-energy signatures. However, as discussed in the preceding sections, while all three systems discussed in this chapter are detected in high-energy data, such signatures have not yet emerged in those data. The improved timing solutions presented in this work will also be useful in new investigations of possible high-energy signatures. Comparing with more BWPs and other pulsar systems will give a clearer picture of what is the most important factor for why a BWP system is stable or unstable.

Bibliography

Alpar M. A., Cheng A. F., Ruderman M. A., Shaham J., 1982, Nature, 300, 728

Archibald A. M., et al., 2009, Science, 324, 1411

Arzoumanian Z., Fruchter A. S., Taylor J. H., 1994, ApJ, 426, 85

Arzoumanian Z., et al., 2018, preprint, (arXiv:1801.01837)

Bassa C. G., et al., 2014, MNRAS, 441, 1825

Bates S. D., et al., 2011, MNRAS, 416, 2455

Bhattacharya D., van den Heuvel E. P. J., 1991, Phys. Rep., 203, 1

Bochenek C., Ransom S., Demorest P., 2015, ApJ, 813, L4

Breton R. P., et al., 2013, ApJ, 769, 108

Chen H.-L., Chen X., Tauris T. M., Han Z., 2013, ApJ, 775, 27

Desvignes G., Barott W. C., Cognard I., Lespagnol P., Theureau G., 2011, in Burgay M., D'Amico N., Esposito P., Pellizzoni A., Possenti A., eds, American Institute of Physics Conference Series Vol. 1357, American Institute of Physics Conference Series. pp 349–350,

Desvignes G., et al., 2016, MNRAS, 458, 3341

Folkner W. M., Williams J. G., Boggs D. H., 2009, Interplanetary Network Progress Report, 178, 1

Fruchter A. S., Stinebring D. R., Taylor J. H., 1988, Nature, 333, 237

Gentile P. A., et al., 2014, ApJ, 783, 69

Guillemot L., et al., 2016, A&A, 587, A109

Hessels J. W. T., et al., 2011, in Burgay M., D'Amico N., Esposito P., Pellizzoni A., Possenti A., eds, American Institute of Physics Conference Series Vol. 1357, American Institute of Physics Conference Series. pp 40–43 (arXiv:1101.1742)

Hewish A., Bell S. J., Pilkington J. D. H., Scott P. F., Collins R. A., 1968, Nature, 217, 709

Hobbs G. B., Edwards R. T., Manchester R. N., 2006, MNRAS, 369, 655

Karuppusamy R., Stappers B., van Straten W., 2008, PASP, 120, 191

Lange C., Camilo F., Wex N., Kramer M., Backer D. C., Lyne A. G., Doroshenko O., 2001, MNRAS, 326, 274

Lazaridis K., et al., 2011, MNRAS, 414, 3134

Lazarus P., Karuppusamy R., Graikou E., Caballero R. N., Champion D. J., Lee K. J., Verbiest J. P. W., Kramer M., 2016, MNRAS, 458, 868

Lee K. J., Wex N., Kramer M., Stappers B. W., Bassa C. G., Janssen G. H., Karuppusamy R., Smits R., 2011, MNRAS, 414, 3251

Lentati L., et al., 2015, MNRAS, 453, 2576

Lorimer D. R., Kramer M., 2012, Handbook of Pulsar Astronomy

Manchester R. N., 2017, in Journal of Physics Conference Series. p. 012001 (arXiv:1801.04323)

Ng C., et al., 2014, MNRAS, 439, 1865

Papitto A., et al., 2013, Nature, 501, 517

Polzin E. J., et al., 2018, MNRAS, 476, 1968

Ransom S. M., et al., 2011, ApJ, 727, L16

Ray P. S., et al., 2012, preprint, (arXiv:1205.3089)

Reynolds M. T., Callanan P. J., Fruchter A. S., Torres M. A. P., Beer M. E., Gibbons R. A., 2007, MNRAS, 379, 1117

Roberts M. S. E., 2011, in Burgay M., D'Amico N., Esposito P., Pellizzoni A., Possenti A., eds, American Institute of Physics Conference Series Vol. 1357, American Institute of Physics Conference Series. pp 127–130 (arXiv:1103.0819)

Roberts M. S. E., 2013, in van Leeuwen J., ed., IAU Symposium Vol. 291, Neutron Stars and Pulsars: Challenges and Opportunities after 80 years. pp 127–132 (arXiv:1210.6903)

Roy J., et al., 2015, ApJ, 800, L12

Schroeder J., Halpern J., 2014, ApJ, 793, 78

Shaifullah G., et al., 2016, MNRAS, 462, 1029

Stappers B. W., Bessell M. S., Bailes M., 1996, ApJ, 473, L119

Stappers B. W., Bailes M., Manchester R. N., Sandhu J. S., Toscano M., 1998, ApJ, 499, L183

Stappers B. W., van Kerkwijk M. H., Bell J. F., Kulkarni S. R., 2001, ApJ, 548, L183

Tielens A. G. G. M., 2009, Astrophysics and Space Science Proceedings, 10, 271

Torres D. F., Ji L., Li J., Papitto A., Rea N., de Oña Wilhelmi E., Zhang S., 2017, ApJ, 836, 68

Verbiest J. P. W., et al., 2016, MNRAS, 458, 1267

van Kerkwijk M. H., Breton R. P., Kulkarni S. R., 2011, ApJ, 728, 95

van Straten W., Demorest P., Oslowski S., 2012, Astronomical Research and Technology, 9, 237